Electrokinetic particle aggregation patterns in microvortices due to particle-field interaction

Diana Hou and Hsueh-Chia Chang[a)]
Department of Chemical and Biomolecular Engineering, Center for Microfluidics and Medical Diagnostics, University of Notre Dame, Notre Dame, Indiana 46556

(Received 14 March 2006; accepted 14 June 2006; published online 12 July 2006)

A complex and dynamic particle banding phenomenon in an electric field is reported. A single cylindrical vortex flow is generated by a dc-biased ac electro-osmotic flow on parallel electrodes. Charged particles are attracted to the vortex by positive dielectrophoresis (DEP) to form rotating cylindrical structures. As the particle concentration increases, the cylinder undergoes longitudinal symmetry breaking, producing concentrated rotating bands caused by field screening effects. The focusing of the particles into bands is shown to obey negative diffusion dynamics of a long-wave instability. Funnels and butterfly-like patterns also form because of secondary longitudinal DEP forces from nonuniform screening effects. © *2006 American Institute of Physics*.
[DOI: 10.1063/1.2221348]

Pattern formation phenomena unique to suspensions are usually driven by particle/fluid inertia and elastic or inelastic particle collisions for large and fluidized granular flows.[1] These suspension instabilities involve complex flow and particle patterns. In contrast, there are few examples of particle segregation and aggregation dynamics at microflow conditions with negligible particle and fluid inertia. These exceptions at Stokes flow conditions are generally believed to be due to viscous fingering instabilities caused by particle concentration variations[2] or by shear-induced migration.[3–5]

Pattern formation of suspensions is, however, quite ubiquitous in the presence of a dc or ac electric field. These fields can induce particle dipoles and hence concentrate charged and uncharged particles dielectrophoretically (DEP) at regions of high or low field intensity.[6,7] The induced dipoles can cause the particles to self-assemble after they are concentrated.[8] Electrophoretic force can also concentrate charged particles against a surface. In some recent examples, such dielectrophoretic and electrophoretic particle motions have been coupled with complex ac electro-osmotic vortex flows to trap particles along stagnation lines on the electrodes.[9–11] When the DEP force on the particle is countered by the gravitational force, the ac electro-osmotic flow can even trap the particles along a levitated line above the electrodes.[12]

However, particle patterns in electrokinetics are generally static and are imprints of the topologies of the flow and electric fields. There has been no report of dynamic and symmetry-breaking particle patterns in an electric field, similar to those in high-inertia granular flows. Without fluid and particle inertia, such intrinsic particle instabilities must necessarily rely on the field-distortion effects of the particles and hence constitute higher-order instabilities that are concentration-dependent.

We report an intrinsic and dynamic microparticle pattern formation phenomenon that breaks the symmetries of both the applied electric field and the ac electro-osmotic (ACEO) flow. The ACEO flow is an electro-osmotic flow driven by microfabricated electrodes, with the dimensions as shown in the schematic of Fig. 1. This flow is housed in a microwell that is enclosed at the top with a transparent plastic layer. The microelectrode pair, comprised of Ti/Au, was fabricated by standard lithography techniques on a silicon wafer. The liquid used is deionized water, which has a Debye screening length of $\lambda \sim 1$ μm. Due to the ac potential imposed on the electrodes, polarized double layers of thickness λ and of opposite charge develop on the electrodes. The localized tangential Maxwell force within the double layer produces a net time-averaged slip velocity on the electrode surface despite the ac nature of the applied field.[13] Because the tangential field is not uniform or even in the same direction, recirculating vortices are generated above the electrodes. Typically, four vortex cylinders are generated, two on each electrode.[10,11] However, with a +1 V dc bias on the left electrode and a grounded right electrode, we are able to sustain a unidirectional slip velocity on both electrodes and generate a single cylindrical flow that spans both electrodes along the x direction, as depicted in Fig. 1.[14] The linear velocity within the vortex can approach 100 μm/s due to the large Maxwell force generated by the 3 V_{pp} of the ac electric field. When the ac field is coupled with a negative bias, the cylindrical flow persists but its direction is reversed. Despite the large fluid velocities, particle and fluid inertia remains negligible due to the small particle and vortex dimensions.

Latex particles, 5–15 μm in diameter, are suspended in deionized water at concentrations of approximately 10^6 and 10^7 particles/ml. These latex particles have an inherent small negative charge, however they are observed to remain within the vortex despite the Coulombic attraction of the positively charged electrode. In the absence of a stagnation line on the electrodes, the large unidirectional surface slip velocity of Fig. 1 prevents any accumulation of the particles on the electrode. To verify this, an electrode array with surface stagna-

[a)]Author to whom correspondence should be addressed. Electronic mail: hchang@nd.edu

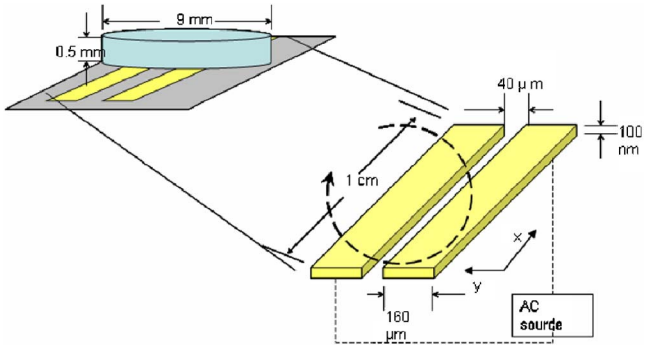

FIG. 1. Electrode configuration used to generate microvortices, where the dashed line represents flow direction. A positive dc bias is applied to the left electrode in the figure. The parallel planar electrode configuration produces a vortex flow observed as a rotating cylinder along the length of the electrode with coordinate x.

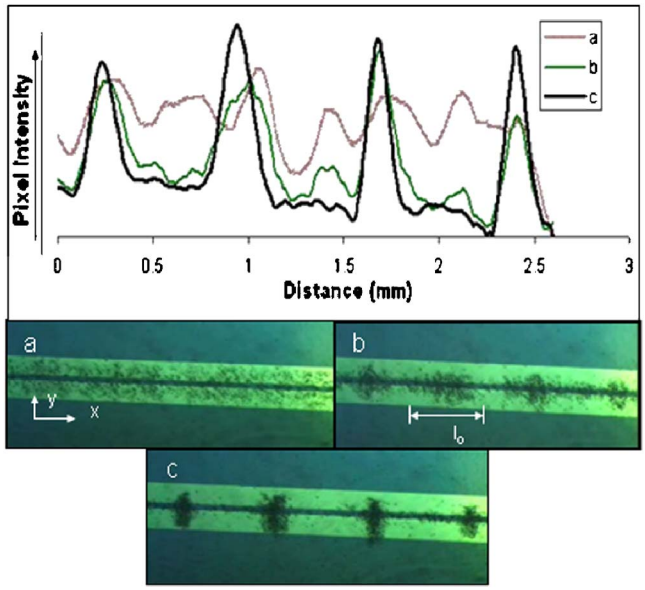

FIG. 2. Breakup of a particle cylinder into concentrated bands above two parallel electrodes under an ac field coupled with a dc bias. A positive dc bias is applied to the top electrodes in the figures. The times elapsed for (b) and (c) are 90 and 135 s, respectively. Initial particle distribution within the cylinder is shown by (a). The solution consists of 5 μm latex particles suspended in deionized water at 10^6 particles/ml. The applied ac peak-peak voltage is 3 V, 5 kHz, coupled with a +1 V dc bias. The estimated initial bandwidth l_o for this sequence is shown in (b). The bandwidth as a function of time is then recorded subsequent to this frame. The pixel intensity along the x axis of Fig. 1, averaged over a 5-s interval of each image, is shown in the left column. An evolution from white noise to a periodic structure is clearly evident.

tion flows is fabricated of Ti/Au on a silicon wafer, as shown in Fig. 4(a). The array is configured such that there is a 40 μm gap between the 160 μm wide electrodes. A dc bias is applied only on every other electrode and the remaining electrodes are always grounded. Due to the existence of alternating charged or uncharged electrodes in this symmetric geometry, the converging and diverging stagnation flows can be created on each electrode surface.[14] Under a 2 V_{pp}, and a 5 kHz ac field coupled with a +1 V dc bias, the vortices flow in the direction such that they generate a converging flow stagnation line on the charged electrode surface and the particles are swept and trapped there by convection. In the following image, the dc bias is changed to a −1 V dc bias and the direction of flow is reversed. The particles are then rapidly swept from the electrode surface, as seen by the dark cloud of particles in Fig. 4(a). The images are taken within 1 s of applying the negative dc bias. Thus, for the isolated electrode pair of Fig. 1, where there is no converging stagnation flow on either electrode, the particles will not trap and will instead remain suspended within the vortex.

The induced particle dipole due to the ac field produces a positive DEP particle flux toward the electrodes, where the particles are then swept by the stronger ACEO vortex flow of Fig. 1 to form the striking hollow cylindrical structure of Fig. 2 that rotates at a constant angular velocity of about 100 μm/s. The levitated and rotating cylinder is observed for both positive and negative bias and is independent of the direction of gravity (examined by inverting the wafer).

The hollow cylinder that appears is because of the large difference between the ACEO velocity and the particle DEP velocity. DEP forces are produced by the nonuniform electric field that generates a field-induced dipole and finite field intensity gradient across the particle. The DEP particle velocity scales as $U_{\mathrm{DEP}} \sim \varepsilon a^2 \nabla |E|^2/\mu$, where ε is the dielectric permittivity, E is the electric field, a is the particle radius, and μ is the fluid viscosity.[6] For the current setup, the U_{DEP} is typically of the order of 1–10 μm/s for the 5–15 μm particles employed. This velocity is much smaller than the flow velocity of 100 μm/s. We have selected the ac frequency range of 5–50 kHz in order to be below the crossover frequency of the latex particles[6] such that they exhibit positive DEP behavior (migration toward the high-field region).

The DEP particle force is initially uniform along the length of the electrodes for the initial homogeneous hollow cylinder of particles. However, as more particles accumulate, a banding instability develops to break up the cylinder into banded structures, as seen in Fig. 2. The band formation is independent of the gap width of the electrodes but the formation time and the band spacing are sensitive to the initial particle concentration. For a more quantitative measurement of the band formation dynamics, we record the pixel intensity along a longitudinal line through the band continuously in time. For better resolution, the pixel reading is averaged over 5 s, which is much shorter than the characteristic time of the evolution dynamics. The intensity profiles of the banded structures are shown in the above the images in Fig. 2. The evolution from white noise to periodically spaced bands is evident.

During the formation of these banded structures, we do not detect any longitudinal variation in the rotating speed, suggesting that viscous effects as in viscous fingering are not at play. This secondary instability occurs only after a sufficient number of particles have accumulated on the particle cylinder, indicating that it is driven by a high-concentration effect. Because of the low permittivity of the latex particles, the concentrated ring is expected to confine the electric field to the electrode surface beneath the ring of particles, thus increasing the local field near the electrode surface but decreasing the field in the bulk. Slight concentration fluctua-

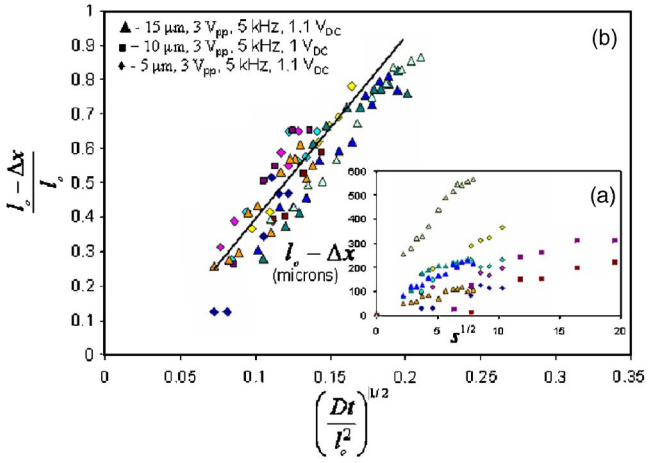

FIG. 3. The measured bandwidth Δx in micrometers, as a function of time in seconds, is scaled according to the theoretical analysis for different particle size, ac peak-peak voltage, ac frequency, and dc bias as indicated in the legend. The particle concentration is held constant at 10^6 particles/ml for all the experiments. Different experiments of identical conditions can produce different initial bandwidths l_o and these data points are represented by the same symbol, but with a different shading. (a) Measured bandwidths plotted against diffusive time. (b) Collapsed data of the subplot by using the diffusivity scaling. The field E_0 is taken to be 750 V/cm and the concentration ϕ ranged between 10 and 30%, with ϕ measured by pixel intensities.

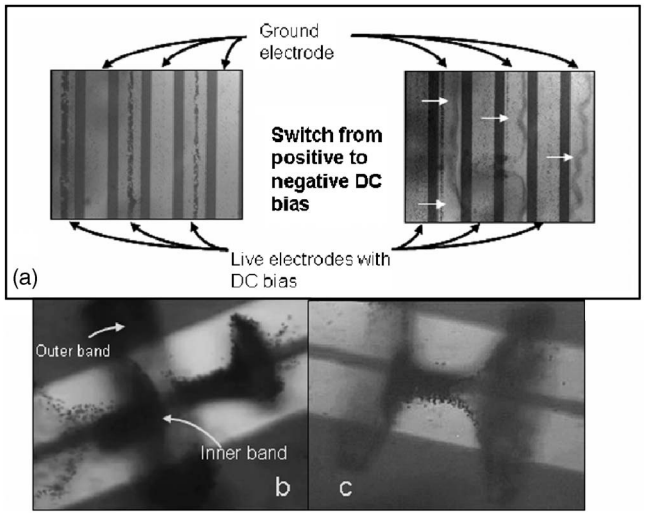

FIG. 4. (a) Particles at concentrations of 10^6 particles/ml are trapped on the electrode surface by a converging flow stagnation line in an ac field of 3 V_{pp} at 5 kHz with a +1 V dc bias. When switched to a −1 V dc bias, the direction of flow reverses and the particles are rapidly swept to the opposite electrode, in the second frame, as seen by the dark cloud of particles, taken 1 s later, indicating the strength of the convective flow. Complex ring structures for exactly the same conditions as (a) but for the single electrode pair of Fig. 1 are observed in (b) and (c) due to confined field and secondary DEP effects. In (b), an inner ring of particles is interlaced within the original banded structure and the inner ring is pulled out to form cones. (c) Merging funnel vortices with an inner ring of particles are drawn out of both vortices to form a butterfly structure. [(b) is enhanced online.]

tions visible in Fig. 2(b) would produce enhanced fields at the high concentration regions. A longitudinal DEP particle flux would then be driven toward these high positive field regions, thus producing a positive feedback and destabilize the original homogeneous cylinder. The equidistant separation of the banded structures indicates a possible instability where a selected wavelength is apparent and requires further study. For simplicity, we choose to analyze only the initial focusing of a single band and not the higher-order wavelength selection mechanism.

The enhanced field as a function of the local particle concentration can be modeled as $E_o(1+\alpha\phi)$, where α is an unknown screening constant and ϕ is the particle volume fraction. The longitudinal DEP particle flux, $U_{\mathrm{DEP}}\phi$, then produces the longitudinal particle balance after linearization about the homogeneous volume fraction, $\partial\phi/\partial t = -D(\partial^2\phi/\partial x^2)$, where $D \sim 2\varepsilon a^2 E_o^2 \phi_o \alpha/\mu$ is a positive diffusivity-like coefficient. With this negative diffusivity, $-D$, the bandwidth of a single band, Δx, should scale as $l_o - \Delta x \sim (Dt)^{1/2}$, where l_o is the initial bandwidth corresponding to $t=0$, taken after some transients have expired. A higher (fourth) order term in $\partial/\partial x$ would produce a high-wave-number cutoff and a selected wavelength. However, the initial focusing of the bands with disturbances having long longitudinal length scales do not involve this higher-order term and we shall delegate it to future studies.

Band formation dynamics were monitored for latex particles of 5, 10, and 15 μm at concentrations of 10^7 particles/ml that were suspended in deionized water. Bandwidths are measured as the band formation progresses, by evaluating the average standard deviation of the peaks of the recorded pixel intensity profiles shown in Fig. 2. Due to the width of the initial band being highly dependent on the initial particle concentration, the widths plotted are subtracted from the initial value l_o at the first recognizable particle concentrations, such as in Fig. 2(b). A plot of the widths of the banded structures as a function of time is depicted in Fig. 3(a). Larger particles with higher DEP mobility tend to have faster dynamics but the pattern formation time is also highly sensitive to the initial particle distribution within the cylinder. For example, symmetry breaking of the cylinders into banded structures required more time for the 10 μm particles than the 5 and 15 μm suspensions because of an uneven initial distribution of particles in the cylinder. Such effects of the initial distribution are minimized by selecting a well-developed l_o. Although a negative diffusive scaling, $l_o - \Delta x \sim t^{1/2}$, is observed at large times for most runs, bands with different diffusivities approach different slopes. However, after normalization by their respective diffusivities, $D \sim 2\varepsilon a^2 E_o^2 \phi_o \alpha/\mu$, and after dividing by l_o to produce dimensionless quantities, the evolution data for the bandwidth for three different particle sizes collapse to a straight line with a slope that is roughly 5, as seen in Fig. 3(b), indicating the correct mechanism for the band formation has been captured. The collapse indicates that the band formation dynamics of larger particles are faster than the smaller particles, as is consistent with visual observation.

A secondary effect resulting from the confined field is observed at very high initial particle concentrations ($>10^6$ particles/ml). The field screened by the first ring of particles can hence sustain another inner ring, whose equilibrium levitation height from the electrode is larger due to the weakened DEP force. These additional ring structures appear within the original banded structures to form concen-

tric cylinders, as seen in Fig. 4(b). In highly concentrated banded structures, the particles in the innermost region of the cylinder will experience a secondary longitudinal field gradient due to the screening by the finite-length outer band. These inner-ring particles are drawn out of the outer band by the higher field outside. The resulting patterns resemble stretching funnels and cones. The merging of funnels from adjacent concentric bands results in the complex butterfly structures seen in Fig. 4(c). These higher-order symmetry-breaking bifurcations epitomize the rich variety of radial and longitudinal pattern dynamics of the current system whose underlying field-screening mechanisms are distinct from other reported suspension instabilities.

This research is supported by a NASA grant and an NSF grant.

[1] J. Li, I. S. Aranson, W.-K. Kwok, and L. S. Tsimring, "Periodic and disordered structures in a modulated gas-driven granular layer," Phys. Rev. Lett. **90**, 134301 (2003).
[2] M. Tirumkudulu, A. Tripathi, and A. Acrivos, "Particle segregation in monodisperse sheared suspensions," Phys. Fluids **11**, 507 (1999).
[3] D. Leighton and A. Acrivos, "The shear-induced migration of particles in concentrated suspensions," J. Fluid Mech. **181**, 415 (1987).
[4] R. Phillips, R. Armstrong, R. Brown, A. Graham, and J. Abbot, "A constitutive equation for concentrated suspension that accounts for shear-induced particle migration," Phys. Fluids A **4**, 30 (1992).
[5] R. Zhou and H.-C. Chang, "Capillary penetration failure of blood suspensions," J. Colloid Interface Sci. **287**, 647 (2005).
[6] H. A. Pohl, *Dielectrophoresis* (Cambridge University Press, London, 1978).
[7] S. K. Thamida and H.-C. Chang, "Nonlinear electrokinetic ejection and entrainment due to polarization at nearly insulated wedges," Phys. Fluids **14**, 4315 (2002).
[8] M. Trau, D. A. Saville, and I. A. Aksay, "Field-induced layering of colloidal crystals," Science **272**, 706 (1996).
[9] N. G. Green, A. Ramos, A. Gonzalez, H. Morgan, and A. Castellanos, "Fluid flow induced by nonuniform AC electric fields in electrolytes on microelectrodes. I. Experimental measurements," Phys. Rev. E **61**, 4011 (2000).
[10] J. Wu, Y. Ben, D. Battigelli, and H.-C. Chang, "Long-range AC electroosmotic trapping and detection of bioparticles," Ind. Eng. Chem. Res. **44**, 2815 (2005).
[11] A. Ramos, H. Morgan, N. G. Green, and A. Castellanos, "AC electric-field induced fluid flow in microelectrodes," J. Colloid Interface Sci. **217**, 420 (1999).
[12] I. Tuval, I. Mezic, F. Bottausci, Y. T. Zhang, N. C. MacDonald, and O. Piro, "Control of particles in microelectrode devices," Phys. Rev. Lett. **95**, 236002 (2005).
[13] A. Gonzalez, A. Ramos, N. G. Green, A. Castellanos, and H. Morgan, "Fluid flow induced by nonuniform AC electric fields in electrolytes on microelectrodes. II. A linear double-layer analysis," Phys. Rev. E **61**, 4019 (2000).
[14] J. Wu, Y. Ben, and H.-C. Chang, "Particle detection by electrical impedance spectroscopy with asymmetric-polarization AC electroosmotic trapping," Microfluid and Nanofluid **1**, 161 (2005).